Hindawi
Mathematical Problems in Engineering
Volume 2022, Article ID 8260169, 13 pages
https://doi.org/10.1155/2022/8260169

Research Article

Collaborative Control Technology of Crosscut Floor Heave in Soft Rocks under Deep High Horizontal Stress

Hongyang Liu,[1,2] **Chengwei Liu**,[1] **Minghua Zhai**,[2] **Peng Zhang**,[1] **Longjiang Wang**,[3] **Feng Wang**,[2] **and Jiangang Liu**[1]

[1]*School of Mining and Mechanical Engineering, Liupanshui Normal University, Liupanshui 553004, Guizhou, China*
[2]*College of Energy and Mining Engineering, Shandong University of Science and Technology, Qingdao 266590, Shandong, China*
[3]*Planning and Construction Department of Heze High-tech Zone Management Committee, Heze 274047, Shandong, China*

Correspondence should be addressed to Chengwei Liu; liuchengwei12@126.com

Received 29 June 2022; Revised 18 August 2022; Accepted 23 August 2022; Published 13 September 2022

Academic Editor: Fuqiang Ren

The repair rate of deep permanent roadways is about 90%, and most of which are projects treating floor heave. The deformation behaviors of crosscut were analyzed in the work according to a trackage crosscut at the shaft station of Panyidong Coal Mine in Huainan, China. Crosscut has complex characteristics such as globality, difference, and rheology under deep stress because that crosscut passes through multiple strata. The mechanism of crosscut floor heave was studied based on on-site in situ stress tests and surrounding rock composition tests. The floor heave of trackage crosscut is water swelling in the mudstone and sandy-mudstone areas where the mineral components are mainly kaolinite and illite mixed layers. In the areas of fine and medium-fine sandstone, trackage crosscut is in shear dislocation under high horizontal stress. The slip-line field theory was used to study the ultimate load and maximum failure depth of crosscut floor heave. According to the deformation characteristics of crosscut floor heave, a collaborative control technology enhancing the bearing structure of all-sided surrounding rocks was proposed, including filling of the U-shaped steel supports, shallow grouting in the all-sided surrounding rocks and deep grouting in the floor and inverted arches. A support scheme for repairing the floor was designed based on the specific engineering geology of trackage crosscut floor heave at the shaft station of the Panyidong Coal Mine. After repairing, the crosscut floor heave was monitored for 70 d. The results showed the following. (1) After repairing, the maximum cumulative floor heave was 45.3 mm, which was only 8.1% of that before repairing. (2) Crosscut floor heave changed greatly within one week after repair, with a maximum floor heave speed of 4.7 mm/d. The floor heave speed was maintained below 1 mm/d after 40 d, and the floor heave tended to be stable after 60 d. The collaborative control technology enhancing the bearing structure of all-sided surrounding rocks could control the crosscut floor heave in soft rocks under deep high horizontal stress.

1. Introduction

Coal plays a fundamental role in China's energy security strategy [1, 2]. China's total energy consumption reached 5.24 billion tons of standard coal in 2021, an increase of 5.2% over the previous year. The annual coal output of 4.07 billion tons hit a new high, an increase of 4.7% over the previous year. With the increased energy demand and mining intensity, the mining depth of coal resources is increasing at a rate of 10–25 m/*a* [3–5]. The underground rock masses show the characteristic of "three highs and one disturbance" (high in situ stress, high geo-temperature, high karst water pressure, and a strong mining disturbance), and roadways have large deformation, strong rheology, serious damage, and difficulty in supporting [6, 7]. According to statistics, the repair rate of deep permanent roadways is 90%, and most of which are floor heave-treating projects. The floor heave accounts for 2/3 to 3/4 of the roof-to-floor convergence of the roadways, which seriously affects the ventilation, transportation, and personnel passage of the mine [8–10]. Most roadways only support the roof and two sides instead of the floor, which is the most vulnerable part of the

surrounding rock-bearing structure. The floor strata bend and expand under extrusion on both sides, the stress of original rock masses, bearing pressures, and physical and mechanical properties of water and floor, thus, forming a floor heave [9].

The mechanism and deformation characteristics of floor heave are complex due to the complexity of surrounding rock properties, stress environment, and occurrence conditions [11–14]. Scholars have studied the formation, mechanism, and influencing factors of floor heave over the years [15–18]. For example, Ma et al. summarized the mechanism of floor heave under various factors and divided it into types of squeeze flow, flexural fold, shear dislocation, and water swelling. The main factors affecting the floor heave of roadways are floor lithology, surrounding-rock stress, hydraulic effect, and support strength [19]. Malkowski P. *et al.* analyzed the in situ measurement data of floor heave, the results showed that groundwater and fault zones intersecting the excavations were considered as the key factors that affect floor upheavals [20]. Moreover, for rocks containing water-absorbed minerals such as claystones or mudstones, the presence of water is more likely to increase the floor's propensity to the floor heave [21]. Sun et al. analyzed the roadway's deformation and failure mechanism of different layered rock masses employing the Euler formula, theory of pressure bar stability, Mohr–Coulomb criterion, and the deflection failure mechanical model [22]. Based on the analysis of the main floor heave case of Glencore Bulga underground operations, Sungsoon et al. believed that main high horizontal stress with greater covering depths and certain floor-lithology configuration is likely to contribute to the failures of floor strata [23].

The control methods of floor heave in different situations are also different [24, 25]. Zhang et al. proposed the grouting reinforcement method for the large floor heave of the retained goaf-side gate road [26]. Wang et al. analyzed the influencing factors of the floor heave of the roadways in the fault-fractured zone, including the influence of the fault-fractured zone, the poor quality of floor rock masses, the deterioration of soaked floors, and weak floor supports. A comprehensive support scheme is proposed to optimize all-sided supports using the anchor, reinforcing mesh, shotcreting and concrete-filled steel tube support, and floor supports are strengthened by reinforced-concrete floor beams [27]. Zhang et al. proposed the combined bolting-grouting support technology of all-sided anchor cables and precast-block inverted arches to address the serious floor heave problems of roadways in the complex environment of deep high in-situ stress and weak interlayers [28].

To sum up, the two sides and bottom corners are reinforced with bolts to control the floor heave in shallow roadways rather than in deep roadways [29, 30]. At present, there are two types of reinforcement methods for floors in deep roadways. One is to use the all-sided support method of retractable supports of U-shaped steel with floor arches [31–33], and the other is to use the joint reinforcement method of floor bolts and cables and floor grouting [34–36]. The first method has a significant control effect on the floor heave of weak broken roadways; however, it has high costs, complicated processes, and low efficiency of construction. Therefore, most mines adopt the second method, which solves the problem of the floor heave of roadways under different geological conditions.

The above analysis shows that each mechanism and prevention technology of floor heave is proposed for certain geological conditions due to the complex surrounding rock properties and stress environment of roadways. Besides, although scholars have studied the mechanism and control technology of floor heave by theoretical analysis, numerical simulation, and similar material simulation, there are few studies on the deformation characteristics and mechanism of crosscut floor heave at the shaft station. The main crosscut at the shaft station is responsible for important tasks such as transportation, ventilation, and pedestrians. It is an important channel connecting the main roadways and coal seams and often passes through the inclined coal measure strata with multiple lithologies [37–39]. Therefore, the mechanism of crosscut floor heave cannot be explained by a single type, and a single support technology is unavailable for its control.

The deformation characteristics and occurrence mechanism of crosscut floor heave are more complicated, especially in deep mining. The deformation characteristics and mechanism of deep crosscut floor heave in soft rocks were analyzed by taking a trackage crosscut at the shaft station of Panyidong Coal Mine in China as the research object in the work. A collaborative control technology enhancing the bearing structure of full-sided surrounding rocks was proposed to control strong crosscut floor heave in soft rocks under deep high stress.

2. Project Overview

2.1. Location of the Mine and Engineering Geological Conditions of Crosscut. Pan Yidong Coal Mine is located in Panji District, Huainan, Anhui, China, about 22 km away from the urban area (Figure 1). The ground elevation is +20.1 m to +23.8 m, and the elevation of the level 1 is −848 m, so the depth of the shaft station is 868.1 m to 871.8 m. The main trackage crosscut is located on the west side of the shaft station, with a total length of about 300 m. It is an important transport channel connecting the heavy vehicle line of the shaft station and the −848 m trackage roadway (Figure 2).

The excavated section of the trackage crosscut is located in the coal-bearing rock series of the upper shihezi formation in the Permian, passing through the F32 fault (Figure 3). On the hanging wall of the fault, the surrounding rocks' lithology of the roadway is mainly sandy and fine sandstone. On the footwall of the fault, the lithology *o* is mainly mudstone, coal, sandy mudstone, fine sandstone, and medium-fine sandstone, and the average inclination angle of the strata is about 7.5°. The section shape of the roadway is a straight wall with a semicircular arch, and the size is width × middle height = 5,200 × 4,540 mm. The initial support method is the combined support of 36# U-shaped steels, anchor cables, bolts, and shotcreting on the contour of the roadway, with the floor unsupported (Figure 3).

Figure 1: Location of Panyidong coal mine.

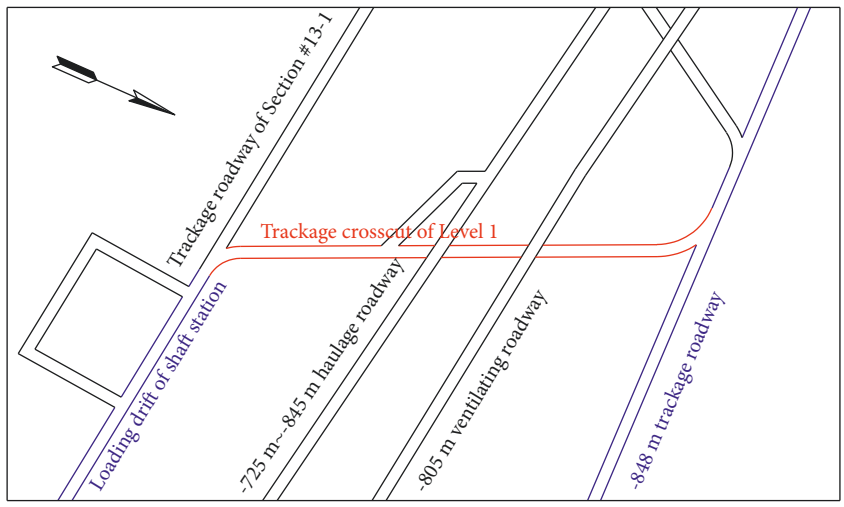

Figure 2: Location of trackage crosscut.

2.2. Characteristics of Crosscut Floor Heave. Obvious floor heave occurred only one month after excavating trackage crosscut. According to the on-site investigation, the deformation of the surrounding rocks of the roadway has the following characteristics.

(1) Globality: all parts of the roadway occurred different degrees of floor heave. The total length of the roadway with floor heave exceeding 100 mm was 210 m, and the maximum uplift reached 280 mm within one month and 560 mm within two months.

(2) Differences: floor heave shows the swelling deformation of mudstone and sandy mudstone (Figure 4(a)); it shows shear-dislocation failure of medium-fine and fine sandstone (Figure 4(b)).

(3) Rheology: the floor heave of the roadway is characterized by the flow deformation over time. As the

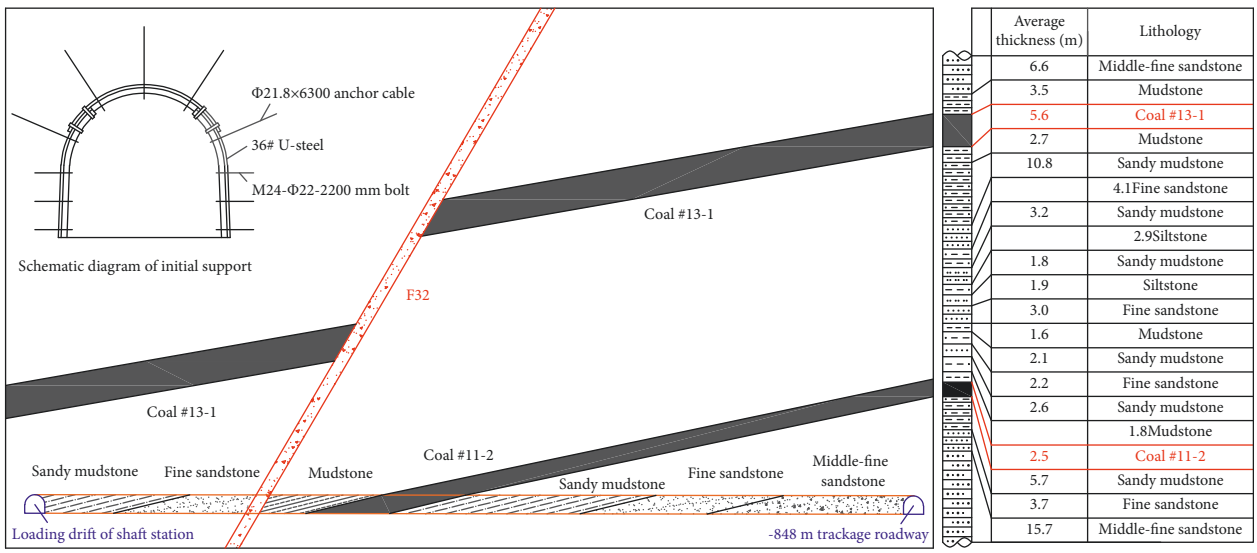

Figure 3: Horizon of trackage crosscut and the comprehensive geological histogram.

(a) (b)

Figure 4: Two types of floor heave. (a) Expansion deformation in the floor. (b) Shear dislocation in the floor.

strata expand and deform to the depth of the floor, the degree of floor heave gradually increases.

3. Mechanism of Crosscut Floor Heave

3.1. Reasons for Crosscut Floor Heave. According to the deformation characteristics of crosscut floor heave, the on-site in-situ stress test, and the laboratory surrounding-rock component test, the reasons for the occurrence of crosscut floor heave are analyzed as follows.

3.1.1. High Horizontal Stress. In situ stress measurements were carried out at three different positions (Measurement station #1~#3 in Figure 5) of trackage crosscut using the stress-relief method. The measuring steps and main devices used by the stress-relief method are shown in Figure 6.

The measurement results (Table 1) show that the maximum principal stress direction is inclined to the horizontal direction. Besides, the overall distribution is east-west and in syncline to the roadway axis. Horizontal stress is greater than the vertical stress, and lateral pressure coefficient λ is about 1.7–1.8. The stability of the surrounding rocks of trackage crosscut is significantly affected by horizontal tectonic stress, and the surrounding rocks of the floor are prone to the floor-heave deformation of shear-slip failure under high horizontal stress. This is the case for the deformation of floor heave in the roadway where surrounding rocks are fine-or medium-fine sandstone.

3.1.2. Mineral Composition of Surrounding Rocks. Four groups of rock samples were selected at the locations with different lithologies in trackage crosscut (Sampling location #1~#4 in Figure 5), and XRD experiments were used to

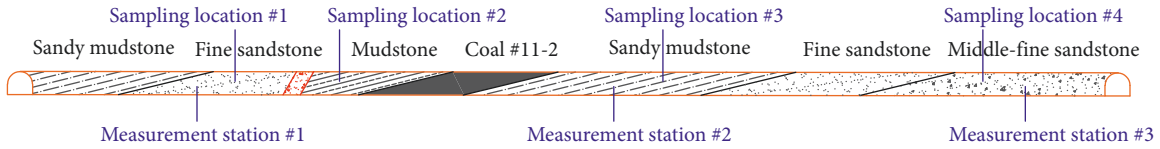

Figure 5: Location of in situ stress measurement and sampled surrounding rocks.

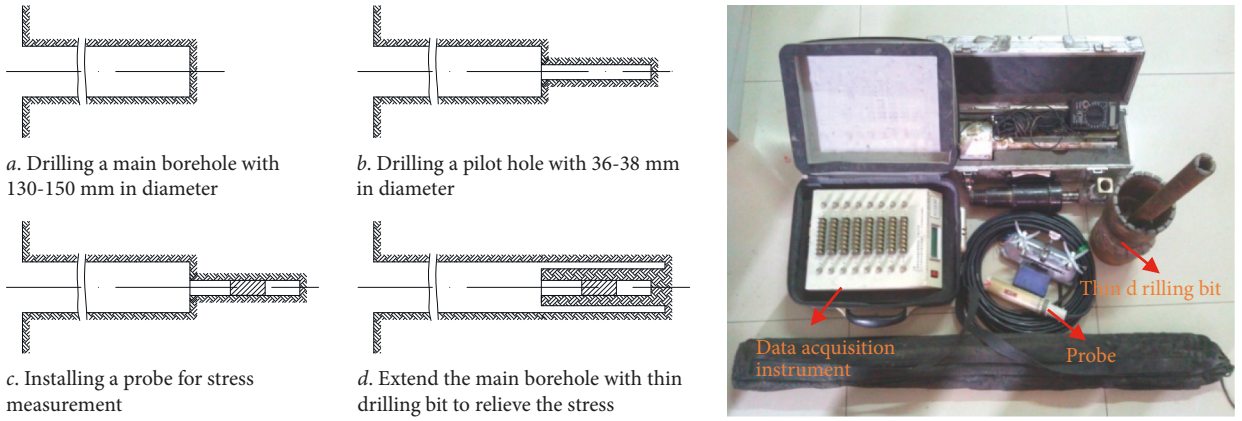

Figure 6: Measuring steps of stress-relief method and the main devices.

Table 1: Measured results of field stress.

Measurement station	Principal stress	Measured results (MPa)	Inclination angle (°)	Azimuth angle (°)
#1	σ_1	33.90	25.3°	183.5°
	σ_2	15.36	64.7°	0.8°
	σ_3	12.73	1.1°	93.0°
	σ_v	18.76		
#2	σ_1	35.82	20.5°	114.3°
	σ_2	20.38	67.5°	320.3°
	σ_3	18.39	9.1°	207.7°
	σ_v	20.99		
#3	σ_1	36.11	11.5°	103.5°
	σ_2	19.13	77.7°	263.4°
	σ_3	18.07	4.1°	12.7°
	σ_v	19.80		

Table 2: Mineral composition contents of rock samples.

Mineral	Rock sample			
	1# fine sandstone (%)	2# mudstone (%)	3# sandy mudstone (%)	4# middle-fine sandstone (%)
Kaolinite	29.5	63.2	43.1	24.7
Quartz	37.6	17.6	25.2	35.2
Illite	7.2	5.6	8.1	6.9
Smectite	2.6	2.4	2.2	2.8
Illite/smectite formation	13.8	7.3	14.7	16.8
Feldspar	1.8	0.4	3.1	2.4
Siderite	4.7		0.3	8.2
Calcite	0.5	0.3	0.3	0.6
Pyrite		0.6	1.1	0.2
Others	Remain	Remain	Remain	Remain

analyze the mineral components of the surrounding rocks. In Table 2, the floor and sandy mudstone are mainly composed of quartz and clay minerals. The kaolinite content reaches 43.1–63.2%, and the total content of illite, montmorillonite, and montmorillonite mixed-layer minerals is about 15.3–25%. In the roadway where the surrounding

rocks of the floor are mudstone and sandy mudstone, the deformation of floor heave occurs with water swelling and becomes more severe under high horizontal stress. It is consistent with the results of field observations.

3.1.3. Low supporting intensity. The surrounding rocks of trackage crosscut are typical soft rocks in deep engineering, but the roadway supports are only supported by U-shaped steels, anchor cables, and bolts. No support measures are taken for the floor, which becomes the outlet for stress release. Therefore, reasonable reinforcement measures need to be taken for the floor.

3.2. Theoretical Calculation of the Ultimate Bearing Capacity and Failure Depth of the Floor. According to the slip-line field theory [40, 41], surrounding-rock stress is redistributed after excavating the underground roadway and the two sides of the roadway form the supporting pressure. If floor rocks are soft, the roadway floor forms a slip-line field under the support pressure of two sides (Figure 7, for the simplified mechanical model).

In Figure 7, areas I, II, and III are called the active stress area, transition area, and passive stress area, respectively; a is the width of the roadway; b the width of the area affected by floor heave; σ_v vertical stress in the area affected by floor heave; $\alpha = \pi/4+\varphi/2$ and $\beta = \pi/4-\varphi/2$; α and β are the angles between the plastic sliding surface and the horizontal plane in areas I and III, respectively, and φ is the internal friction angle of the strata in the floor. It is assumed that the boundaries of the active area and the passive stress area are isosceles triangles to simplify the calculation, and the boundary of the transitioned stress area satisfies the logarithmic-spiral equation. The waist length of the active area is r_0; h is the plastic failure depth at any position of the floor; ω is the included angle between spiral r_0 and r; ξ is the included angle between spiral r and the floor.

It is assumed that the rock masses of the floor are ideal elastic-plastic mediums. When the strata in the floor are unstable and floor heave occurs, the broken rock masses in the floor meet the Hoke–Brown strength criterion [42]:

$$\sigma_1 = \sqrt{m \cdot \sigma_c \cdot \sigma_3 + s \cdot \sigma_c^2} + \sigma_3, \tag{1}$$

where m and s are the parameters related to the rock types and the degrees of crushing of rock masses, respectively, the value range of s is 0~1.0, for intact rocks, $s = 1.0$, σ_c is the uniaxial compressive strength of rocks, and σ_1 and σ_3 are maximum and minimum principal stresses, respectively, when the rock masses are damaged.

Maximum principal stress σ_1^1 in the active stress area is vertical stress transmitted by the coal pillar of the roadway and minimum principal stress is horizontal stress σ_3^1:

$$\sigma_1^1 = \sqrt{m \cdot \sigma_c \cdot \sigma_3^1 + s \cdot \sigma_c^2} + \sigma_3^1. \tag{2}$$

Maximum principal stress σ_1^3 in the passive stress area is the horizontal thrust provided by the active stress area, and

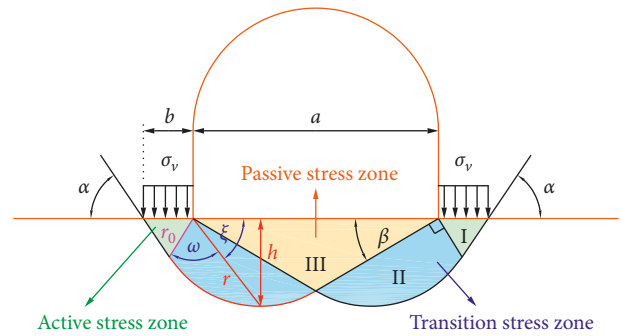

Figure 7: Mechanics model of the floor heave of the roadway.

minimum principal stress σ_3^3 is the free surface stress of the roadway floor, which is equal to 0.

Then,

$$\sigma_1^3 = \sqrt{s} \cdot \sigma_c. \tag{3}$$

When floor heave is about to occur in the roadway, both the active and passive stress areas of the strata on the floor are in the limited equilibrium under vertical stress. At this time, $\sigma_3^1 = \sigma_1^3$. (3) is substituted into (2) to obtain the ultimate load of the rock masses of the floor, denoted as

$$\sigma_1^{\max} = \left(\sqrt{m \cdot \sqrt{s} + s} + \sqrt{s} \right) \sigma_c. \tag{4}$$

When maximum vertical stress σ_v in the area affected by floor heave exceeds the ultimate load of the rock masses in the floor, that is, when $\sigma_v > \sigma_1^{\max}$, the rock masses have floor heave.

The boundary of the transitioned stress area satisfies the logarithmic-spiral equation (26).

Then,

$$r = r_0 \cdot e^{\omega \tan \varphi}. \tag{5}$$

The geometric relationship in Figure 7 shows that failure depth h at any position of the floor is

$$h = r \cdot \sin \xi = r_0 \cdot e^{\omega \tan \varphi} \cdot \sin \xi. \tag{6}$$

From the angle relation in Figure 7,

$$\xi = \frac{\pi}{2} + \beta - \omega = \frac{3\pi}{4} - \frac{\varphi}{2} - \omega. \tag{7}$$

(7) is substituted into (6) to obtain

$$h = r_0 \cdot e^{\omega \tan \varphi} \cdot \sin\left(\frac{3\pi}{4} - \frac{\varphi}{2} - \omega \right). \tag{8}$$

The maximum failure depth $h_{\max}$ of the floor is at $\omega = \pi/4 + \varphi/2$ by taking the derivative of (8) concerning ω:

$$h_{\max} = r_0 \cdot e^{(\pi/4+\varphi/2)\tan \varphi} \cdot \cos \varphi. \tag{9}$$

From the geometric relationship in Figure 7,

$$\cos \alpha = \frac{b}{2r_0}, \quad \cos \beta = \frac{a}{2r}. \tag{10}$$

Since $\alpha = \pi/4 + \varphi/2$ and $\beta = \pi/4 - \varphi/2$, (5), (9), and (10) can be solved simultaneously to obtain

$$h_{\max} = a \cdot e^{(\varphi/2 - \pi/4)\tan\varphi} \cdot \sin\left(\frac{\pi}{4} - \frac{\varphi}{2}\right). \quad (11)$$

The section width of trackage crosscut $a = 5.2$ m; floor frictional angles of the strata in the floor are as follows: $\varphi = 28$, 30, 26, 27, and 23° for mudstone, sandy mudstone, fine sandstone, medium-fine sandstone, and coal, respectively. After substituting into (1), the maximum failure radius of the floor is in the area where the surrounding rocks are coal seams, and $h_{\max} = 2.24$ m.

The height of the heaving area of the floor is measured on-site as $h_0 = 560$ mm, so theoretically, the maximum failure depth of the trackage-crosscut floor is $H = h_{\max} + h_0 = 2.8$ m.

4. Collaborative Control Technology of Crosscut Floor Heave

The above analysis shows that trackage crosscut floor heave belongs to the water swelling-shear dislocation. Control technology of floor heave enhancing the full-section surrounding rock bearing structure is proposed according to its mechanism [18, 32, 33].

4.1. Filling behind U-Shaped Steel Supports. It is inevitable that there are holes in the section formed during entry excavation, which makes the U-steel support and the surrounding rock present random point and line contact, causing the U-steel support to suffer from concentrated load or eccentric load, which reduces the bearing performance of the support. The function of filling behind U-shaped steel supports is that the hole space of the surrounding rock behind the U-steel support is filled with grout to improve the interaction between the surrounding rock and U-shaped steel supports and reduce other inelastic deformations required to achieve the rated resistance of the U-shaped steel supports, conducive to early supporting of U-steels. On the contrary, the injection of grout into the shallow fissures of the surrounding rock can increase the residual strength of the surrounding rock and can effectively prevent the weathering and deliquesce of the argillaceous soft rock.

A pre-embedded T-tube is used for filling (Figure 8). A T-shaped grouting pipe is made of a steel pipe with a wall thickness of 3.25 mm and a diameter of 15 mm, and the grouting section of the T-shaped pipe is buried behind the steel arches. Then, spray 50–80 mm concrete mortars on the roadway surface as a slurry stopper to prevent the outflow of the slurries after filling. Meanwhile, it isolates air and moisture to prevent the corrosion of supporting components such as U-shaped sheds and the water swelling of surrounding rocks rich in clay minerals.

4.2. Shallow Grouting in All-Sided Surrounding Rocks and Deep Grouting in the Floor. Sun et al. proposed a continuous double-shell support of shallow grouting (shallow supporting shell) and deep grouting of anchor cable bundles (deep reinforcing shell) in the floor for the roadways under high horizontal stress [34]. However, the uniformity of the surrounding rock bearing of the roadway is ignored without grouting in all-sided surrounding rocks, which cannot form an effective bearing shell. On this basis, the work proposed the supporting technology of shallow grouting in all-sided surrounding rocks and deep-hole grouting in the floor (Figure 9).

Shallow grouting cements the loose and broken all-sided surrounding rocks into a whole, forming an effective bearing shell, which can resist the deformation and failure of the shallow surrounding rocks in all directions. The deep grouting of the floor has the following advantages, e.g., improving the bearing range of the surrounding rocks, blocking the transfer of deep surrounding rocks' stress to the roadway floor, and protecting the shallow bearing shell.

4.3. Inverted Arch. The inverted arch (Figure 10) can increase the bending resistance of the floor, buffer the long-term damage to the floor caused by high stress, and avoid the plastic flow of the two sides of broken rock masses to the floor [35]. The modifying effect of shallow grouting in all-sided surrounding rocks and deep grouting in the floor on the broken surrounding rocks can control the continuous flow of crosscut floor heave.

5. Engineering Practice and Effect

5.1. Support Scheme of Trackage Crosscut in the Floor. The support scheme for repairing trackage crosscut was designed (Figure 11) according to the maximum failure depth of floor heave calculated in Section 3 and the collaborative control technology in Section 4.

(1) U-shaped steel supports: the 36# U-shaped steel yielding supports were used, and the lap length of each section was 500 mm, with the pre-tightening torque of the clamps not less than 350 N*m*. The distance between the U-shaped steels was 700 mm, and support rods were installed between each row of U-shaped steels. Then, the T-shaped grouting pipes were pre-buried behind the wall for filling.

(2) Bolts: M24-Φ22-2400 mm left-handed high-strength threaded steel bolts without longitudinal bar and grouting bolts were used crosswise. A CK2335 (diameter: 23 mm, length: 35 mm, and gel time: 8~40 s) and a K2360 (diameter: 23 mm, length: 60 mm, and gel time: 41~90 s) anchoring agent were used for each bolt, and the preload was not less than 70 kN.

(3) Anchor cables: Φ21.6 × 6,300 mm anchor cables with the strength of 1864 MPa and grouting anchor cables were used crosswise. A CK2335, a K2360, and a Z2360 (diameter: 23 mm, length: 35 mm, and gel time: 91~180 s) anchoring agent were used for the anchor cable. The design preload was not less than 150 kN.

(4) Inverted arch (Figure 10 for the specific parameters).

Figure 8: Filling behind the frame with the T-shaped grouting tube. (a) Pre-embedded T-tube. (b) The effect after spraying.

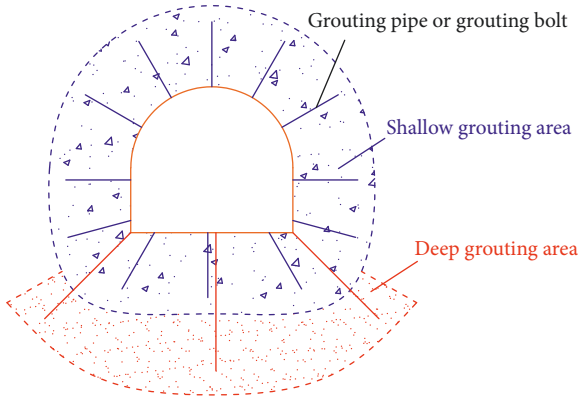

Figure 9: Shallow grouting in all-sided surrounding rocks and deep grouting in the floor.

(5) Spraying layer of concretes: the roof and two sides of C20 concrete layers with a spraying thickness of 150 mm were used to close the surrounding rocks, and the initial spraying thickness was not less than 70 mm. After the bolts and anchor cables were installed, the secondary injection was performed.

(6) Filling: after the roof and the two sides were sprayed with concretes, they could be filled behind the U-shaped steel frames.

(7) Shallow grouting in all-sided surrounding rocks and deep grouting in the floor: after the above procedures were completed, grouting was performed using grouting bolts and grouting anchor cables. The slurries were cement-water glass, and 28.66 L water glass was added to 1 m^3 cement slurry, with the grouting pressure of 3–5 MPa.

5.2. Control Effect of Floor Heave of Trackage Crosscut. After the trackage crosscut was repaired according to the new support scheme, the floor heave mass was monitored at three monitoring stations with different lithologies (Figure 12). There were four monitoring points (A, B, C, and D)

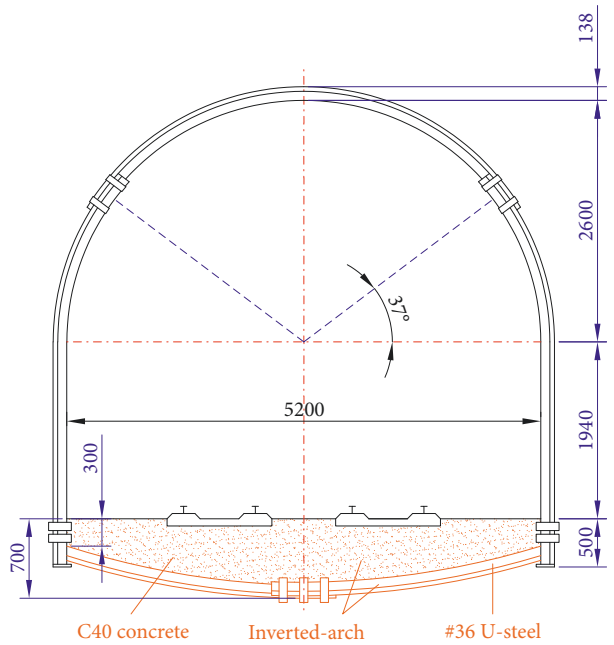

Figure 10: Inverted arch composed of U-shaped steel and concretes.

at each monitoring station, and each monitoring point was a bolt of length of 800 mm, which was fully grouted in the rock mass to avoid movement during the observation period (Figure 13). To determine the convergence, the distance AB, CD, and AD (or BD) was measured with a tape measure or a laser range finder. The floor heave mass variation with time was obtained (Figure 14).

(1) During the monitoring time of 70 days, the cumulative floor heave masses of trackage crosscut of the three stations are 40.2, 45.3, and 35.1 mm, respectively, and the maximum value occurs in the area where the surrounding rocks are coal. During monitoring, the maximum floor heave speeds of the three stations are 4.2, 4.7, and 3.7 mm/d, respectively.

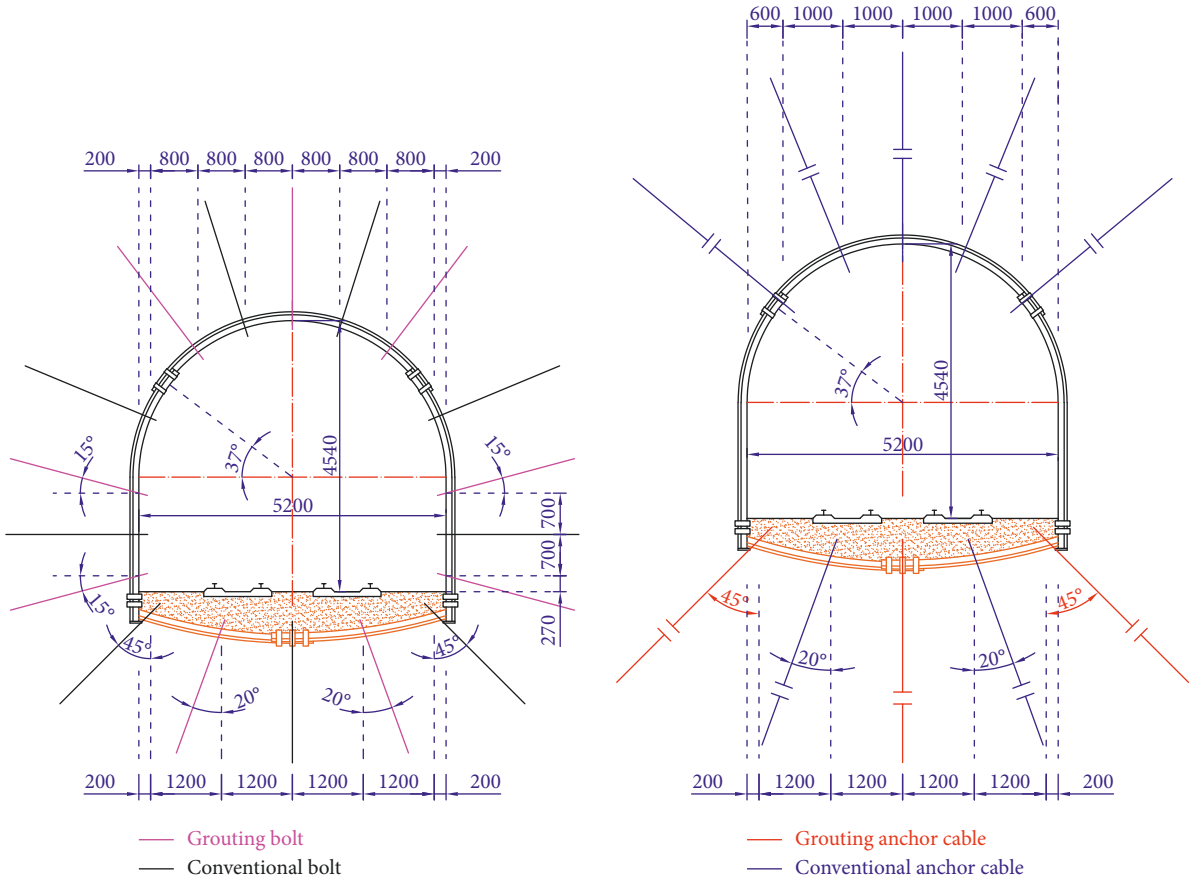

(a)

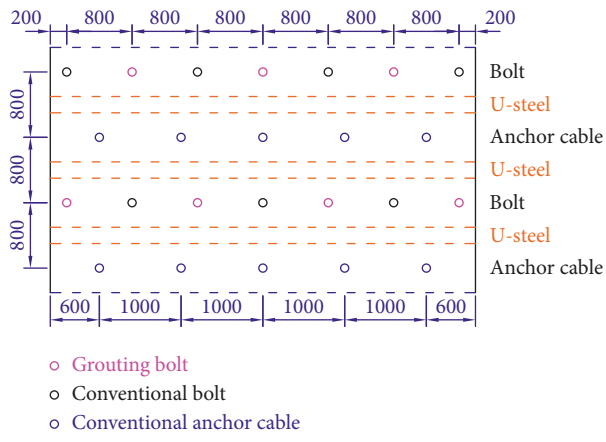

(b)

Figure 11: Continued.

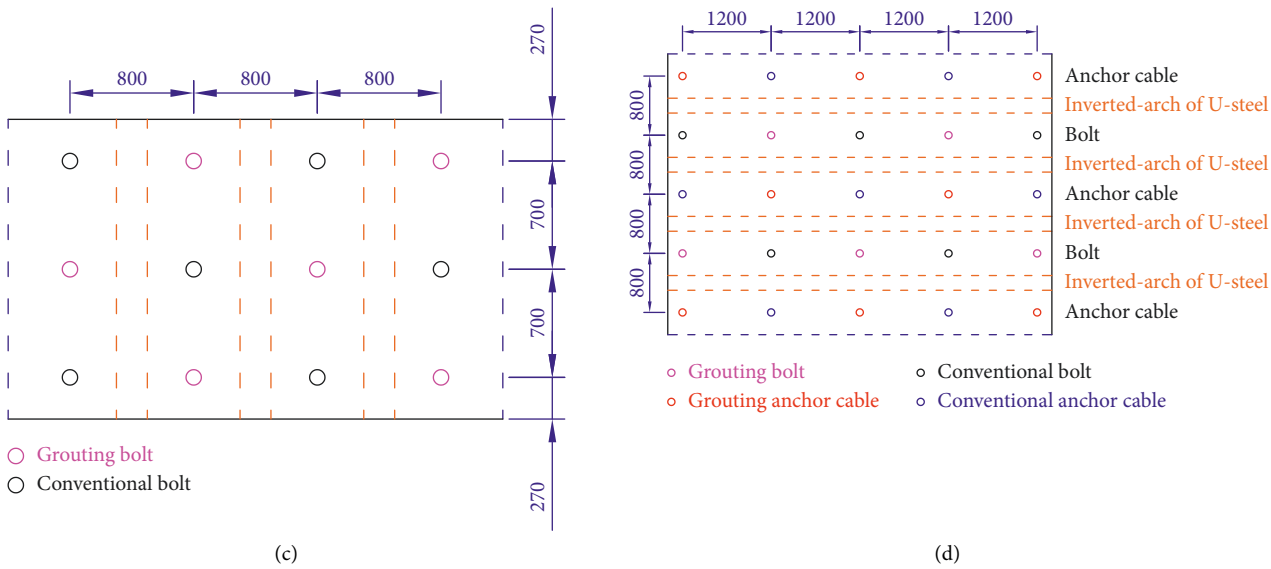

Figure 11: Support scheme of trackage crosscut. (a) Section view of the bolt and anchor cable layouts. (b) Bottom view of the bolt and anchor cable layouts in the roof. (c) Side view of the bolt layout in rib. (d) Top view of the bolt and anchor cable layouts in the floor.

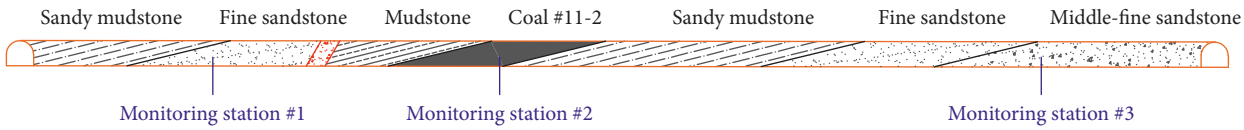

Figure 12: Location of the monitoring station.

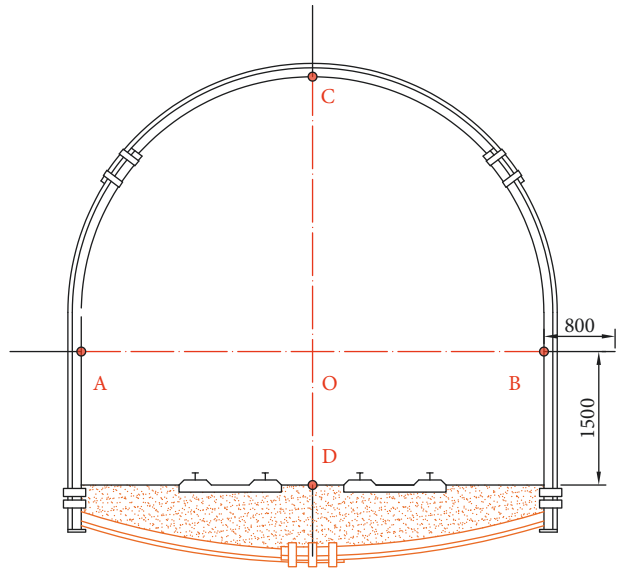

Figure 13: Monitoring station.

The maximum speed also occurs in the areas where the surrounding rocks are coal.

(2) Floor heave changes greatly only within a week after the restoration. After 40 d, the floor heave remained below 1 mm/d. After 60 d, the floor heave speed was close to 0, and the floor heave mass remain unchanged, indicating that the trackage crosscut had become stable at this time.

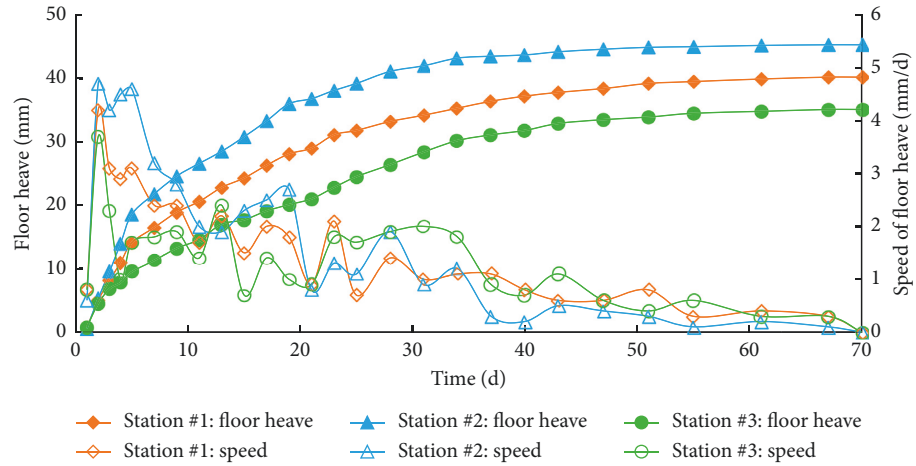

Figure 14: Floor heave curves with time.

After adopting the new support scheme, the maximum floor heave mass is only 8.1% of the maximum mass before restoration. It shows that the control technology enhancing the all-sided surrounding rock bearing structure has a good control effect on crosscut floor heave.

6. Summary and Conclusions

Based on the trackage crosscut at the shaft station of Panyidong Coal Mine, the work studied the control technology of crosscut floor heave under deep high horizontal stress.

(1) Crosscut passed through multiple strata, and the occurrence conditions of surrounding rocks were complicated. Its deformation has complex characteristics such as globality, difference, and rheology under deep high horizontal stress.

(2) Crosscut floor heave showed water swelling in the mudstone and sandy mudstone areas where the mineral components were kaolinite and montmorillonite mixed layers. It presented shear dislocation under high horizontal stress in the areas of fine and medium-fine sandstone.

(3) Based on the slip-line field theory, the ultimate load of crosscut floor heave in the floor strata is $\sigma_1^{\max} = (\sqrt{m \cdot \sqrt{s} + s} + \sqrt{s})\sigma_c$. The maximum failure depth of floor heave without supports is $h_{\max} = a \cdot e^{(\varphi/2 - \pi/4)\tan\varphi} \cdot \sin(\pi/4 - \varphi/2)$. According to the calculation, the maximum failure depth of the unsupported crosscut floor in theory is 2.8 m.

(4) Given the deformation characteristics and mechanism of crosscut floor heave, a collaborative control technology enhancing the all-sided surrounding rock bearing structure was proposed, including the filling of U-shaped steel supports, shallow grouting in all-sided surrounding rocks, and deep grouting in the floor and inverted arches.

(5) According to the trackage crosscut at the shaft station of Panyidong Coal Mine, a support scheme for repairing the floor was designed, and the crosscut floor heave was continuously monitored for 70 d. The results showed the following. (1) After repairing, the maximum cumulative floor heave mass was 45.3 mm, which was only 8.1% of that before repairing. (2) Floor heave changed greatly within one week after repairing, and the maximum floor heave speed was 4.7 mm/d. The floor heave speed was maintained below 1 mm/d after 40 d, and the floor heave mass was stable after 60 d.

Data Availability

All data included in this study can be obtained from the corresponding author upon request.

Conflicts of Interest

The authors declare that there are no conflicts of interest regarding the publication of this paper.

Acknowledgments

This work was supported by the National Natural Science Foundation of China (51778215 and 52174072), the Education Department of Guizhou Province Fund (Qianjiaohe KY Zi [2017] 265, Qianjiaohe KY Zi [2019] 073, Qianjiaohe KY Zi [2020] 050, Qianjiao XKTJ [2020] 23), the Science and Technology Department of Guizhou Province Fund (Qiankehe Platform Talent-YSZ [2021] 001), the Natural Science Foundation of Shandong Province (ZR2021QE170), and the Liupanshui Science and Technology Bureau fund (52020-2018-04–08).

References

[1] X. L. Li, S. J. Chen, Q. M. Zhang, X. Gao, and F. Feng, "Research on theory, simulation and measurement of stress behavior under regenerated roof condition," *Geomechanics and Engineering*, vol. 26, no. 1, pp. 49–61, 2021.

[2] H. Y. Liu, B. Y. Zhang, X. L. Li et al., "Research on roof damage mechanism and control technology of gob-side entry

retaining under close distance gob," *Engineering Failure Analysis*, vol. 138, Article ID 106331, 2022.

[3] H. P. Xie, "Research review of the state key research development program of China: deep rock mechanics and mining theory," *Journal of China Coal Society*, vol. 44, no. 5, pp. 1283–1305, 2019.

[4] X. J. Feng, Z. Ding, Q. J. Hu, X. Zhao, M. Ali, and J. T. Banquando, "Orthogonal numerical analysis of deformation and failure characteristics of deep roadway in coal mines: a case study," *Minerals*, vol. 12, no. 2, p. 185, 2022.

[5] L. Yuan, "Research progress of mining response and disaster prevention and control in deep coal mines," *Journal of China Coal Society*, vol. 46, no. 3, pp. 716–725, 2021.

[6] X. J. Chen, L. Y. Li, L. Wang, and L. L. Qi, "The current situation and prevention and control countermeasures for typical dynamic disasters in kilometer-deep mines in China," *Safety Science*, vol. 115, pp. 229–236, 2019.

[7] P. Wang, N. Zhang, J. G. Kan, B. Wang, and X. L. Xu, "Stabilization of rock roadway under obliquely straddle working face," *Energies*, vol. 14, no. 18, p. 5759, 2021.

[8] P. Gong, Z. G. Ma, X. Y. Ni, and R. R. Zhang, "Floor heave mechanism of gob-side entry retaining with fully-mechanized backfilling mining," *Energies*, vol. 10, no. 12, p. 2085, 2017.

[9] X. P. Lai, H. C. Xu, P. F. Shan, Y. L. Kang, Z. Y. Wang, and X. Wu, "Research on mechanism and control of floor heave of mining-influenced roadway in top coal caving working face," *Energies*, vol. 13, no. 2, p. 381, 2020.

[10] H. S. Jia, L. Y. Wang, K. Fan, B. Peng, and K. Pan, "Control technology of soft rock floor in mining roadway with coal pillar protection: a case study," *Energies*, vol. 12, no. 15, p. 3009, 2019.

[11] Q. Yin, R. C. Liu, H. W. Jing, H. J. Su, L. Y. Yu, and L. X. He, "Experimental study of nonlinear flow behaviors through fractured rock samples after high-temperature exposure," *Rock Mechanics and Rock Engineering*, vol. 52, no. 9, pp. 2963–2983, 2019.

[12] Q. Yin, J. Y. Wu, C. Zhu, M. C. He, Q. X. Meng, and H. W. Jing, "Shear mechanical responses of sandstone exposed to high temperature under constant normal stiffness boundary conditions," *Geomechanics and Geophysics for Geo-Energy and Geo-Resources*, vol. 7, no. 2, p. 35, 2021.

[13] G. Feng, X. C. Wang, M. Wang, and Y. Kang, "Experimental investigation of thermal cycling effect on fracture characteristics of granite in a geothermal-energy reservoir," *Engineering Fracture Mechanics*, vol. 235, Article ID 107180, 2020.

[14] Z. Chun, L. Yun, and F. Gan, "Influence of temperature on quantification of mesocracks: implications for physical properties of fine-grained granite," *Lithosphere*, vol. 2021, Article ID 7824057, 2021.

[15] S. Mo, H. L. Ramandi, J. Oh et al., "A new coal mine floor rating system and its application to assess the potential of floor heave," *International Journal of Rock Mechanics and Mining Sciences*, vol. 128, Article ID 104241, 2020.

[16] X. J. Feng, Z. Ding, Y. Q. Ju, Q. M. Zhang, and M. Ali, "Double peak' of dynamic strengths and acoustic emission responses of coal masses under dynamic loading," *Natural Resources Research*, vol. 31, no. 3, pp. 1705–1720, 2022.

[17] M. Wang, D. J. Zheng, K. W. Wang, and W. F. Li, "Strain energy analysis of floor heave in longwall gateroads," *Royal Society Open Science*, vol. 5, no. 8, Article ID 180691, 2018.

[18] J. G. Kan, G. C. Li, N. Zhang, P. Wang, C. L. Han, and S. Wang, "Changing characteristics of sandstone pore size under cyclic loading," *Geofluids*, vol. 2021, Article ID 6664925, 1–2 pages, 2021.

[19] Z. Q. Ma, Y. D. Jiang, Y. Liu, W. S. Du, and D. Z. Kong, "Investigation on support pattern of a coal mine roadway under dynamic pressure of mining - a case study," *International Journal of Oil, Gas and Coal Technology*, vol. 18, no. 3/4, pp. 402–422, 2018.

[20] P. Malkowski, L. Ostrowski, and L. Bednarek, "The effect of selected factors on floor upheaval in roadways—in situ testing," *Energies*, vol. 13, no. 21, p. 5686, 2020.

[21] P. Malkowski, L. Ostrowski, and J. Stasica, "Modeling of floor heave in underground roadways in dry and waterlogged conditions," *Energies*, vol. 15, no. 12, p. 4340, 2022.

[22] X. M. Sun, P. Y. Miao, F. X. Shen, W. C. Zhao, and M. H. Yang, "Study on floor heave mechanism of horizontal layered soft rock roadway in deep well under different stress states," *Journal of Mining and Safety Engineering*, vol. 35, no. 6, pp. 1099–1106, 2018.

[23] S. Mo, K. Tutuk, and S. Saydam, "Management of floor heave at Bulga Underground Operations-A case study," *International Journal of Mining Science and Technology*, vol. 29, no. 1, pp. 73–78, 2019.

[24] G. Y. Wang and L. Jin, "Study on dynamic responses of roadway controlled by borehole pressure relief and prestressed grouting anchor cable on the floor under dynamic load," *Chinese Journal of Applied Mechanics*, vol. 34, no. 5, pp. 881–886, 2017.

[25] X. Q. Wang, J. G. Kan, and J. K. Jiao, "Mechanism of floor heave in the roadway with high stress and soft rock and its control practice," *Journal of Mining & Safety Engineering*, vol. 34, no. 2, pp. 214–220, 2017.

[26] Z. Y. Zhang and H. Shimada, "Numerical study on the effectiveness of grouting reinforcement on the large heaving floor of the deep retained goaf-side gateroad: a case study in China," *Energies*, vol. 11, no. 4, p. 1001, 2018.

[27] J. Wang, C. C. Hu, and J. P. Zuo, "Mechanism of roadway floor heave and control technology in fault fracture zone," *Journal of China Coal Society*, vol. 44, no. 2, pp. 397–408, 2019.

[28] D. Zhang, J. B. Bai, S. Yan, R. Wang, N. K. Meng, and G. Y. Wang, "Failure mechanism of surrounding rock and control of floor heave in heterogeneous composite rock roadway," *Chinese Journal of Geotechnical Engineering*, vol. 44, no. 9, pp. 1699–1709, 2022.

[29] K. Wang, Y. L. Huang, H. D. Gao et al., "Recovery technology of bottom coal in the gob-side entry of thick coal seam based on floor heave induced by narrow coal pillar," *Energies*, vol. 13, no. 13, p. 3368, 2020.

[30] C. L. Wang, G. Y. Li, A. S. Gao, F. Shi, Z. J. Lu, and H. Lu, "Optimal pre-conditioning and support designs of floor heave in deep roadways," *Geomechanics and Engineering*, vol. 14, no. 5, pp. 429–437, 2018.

[31] J. P. Zuo, Y. J. Sun, and K. Li, "Study of the reinforced supporting length and floor heave control technology of soft rock roadway influenced by collapse column," *Journal of China University of Mining & Technology*, vol. 46, no. 1, pp. 18–26, 2017.

[32] X. Z. Hua and Y. F. Li, "Mechanics analysis on floor deformation of gob-side entry retaining and prevention and control of floor heave," *Journal of China Coal Society*, vol. 41, no. 7, pp. 1624–1631, 2016.

[33] Z. S. Wang, J. Z. Li, J. Lin, L. Yang, and X. Z. Meng, "Mechanism and control technology of floor heave in deep high-stress water-rich clay soft rock roadway," *Coal Science and Technology*, vol. 49, no. 7, pp. 71–78, 2021.

[34] L. H. Sun, B. S. Yang, C. D. Sun, X. Li, and Z. W. Wang, "Experimental research on mechanism and controlling of

floor heave in deep soft rock roadway," *Journal of Mining & Safety Engineering*, vol. 34, no. 2, pp. 235–242, 2017.

[35] X. Z. Hua, M. Yang, Q. J. Liu, and P. Yang, "Model test on evolution mechanism of floor heave in gob-side retaining entry of deep mine," *Journal of Mining & Safety Engineering*, vol. 35, no. 1, pp. 1–9, 2018.

[36] L. H. Sun, B. S. Yang, W. B. Yang, and C. D. Sun, "Reinforcement mechanism and experimental study on continuous double shell of deep roadway," *Journal of Mining & Safety Engineering*, vol. 30, no. 5, pp. 687–691, 2013.

[37] Y. D. Jiang, Y. X. Zhao, W. G. Liu, and Q. Li, "Research on floor heave of roadway in deep mining," *Chinese Journal of Rock Mechanics and Engineering*, vol. 23, no. 14, pp. 2396–2401, 2004.

[38] C. Wang, Y. P. Wu, and X. P. Huang, "Mechanism of floor failure of roadway supported by inverted arch under complicated surrounding rocks and its control," *Journal of Mining & Safety Engineering*, vol. 36, no. 5, pp. 959–976, 2019.

[39] Y. Shuaifeng, M. Haifeng, C. Zhiheng et al., "Permeability enhancement mechanism of sand-carrying hydraulic fracturing in deep mining: a case study of uncovering coal in cross-cut," *Energy Science & Engineering*, vol. 7, no. 5, pp. 1867–1881, 2019.

[40] Z. Z. Zhang, M. Deng, X. Y. Wang, W. J. Yu, F. Zhang, and V. D. Dao, "Field and numerical investigations on the lower coal seam entry failure analysis under the remnant pillar," *Engineering Failure Analysis*, vol. 115, Article ID 104638, 2020.

[41] H. Cheng, H. B. Zhao, J. F. Xu, F. Y. Qin, Y. X. Zhang, and L. F. Hu, "Study on floor heave mechanism and control technology of roadway based on slip line field theory," *Journal of Mining Science and Technology*, vol. 6, no. 3, pp. 314–323, 2021.

[42] H. H. Zhu, Q. Zhang, and L. Y. Zhang, "Review of research progresses and applications of hoek-Brown strength criterion," *Chinese Journal of Rock Mechanics and Engineering*, vol. 32, no. 10, pp. 1945–1963, 2013.